Spatially resolved epigenome-transcriptome co-profiling of mammalian tissues at the cellular level

Rong Fan (✉ rong.fan@yale.edu)

Yale University   https://orcid.org/0000-0001-7805-8059

Di Zhang

Yale University

Yanxiang Deng

Yale University   https://orcid.org/0000-0002-9975-8086

Petra Kukanja

Laboratory of Molecular Neurobiology, Karolinska Institutet   https://orcid.org/0000-0003-1228-5923

Marek Bartosovic

Karolinska Institutet

Graham Su

Yale University

Shuozhen Bao

Yale University

Yang Liu

Yale University

Yang Xiao

Yale University   https://orcid.org/0000-0001-7878-4923

Sai Ma

Broad Institute of MIT and Harvard   https://orcid.org/0000-0002-9785-7929

Gorazd Rosoklija

Columbia University

Andrew Dowrk

Columbia University

J. Mann

Columbia University

Kam Leong

Columbia University

Maura Boldrini

Columbia University   https://orcid.org/0000-0003-3574-7641

Goncalo Castelo-Branco

Karolinska Institutet   https://orcid.org/0000-0003-2247-9393

Biological Sciences - Article

Abstract

Emerging spatial technologies including spatial transcriptomics and spatial epigenomics are becoming powerful tools for profiling cellular states in the tissue context. However, current methods capture only one layer of omics information at a time precluding the possibility to examine the mechanistic relationship across the cental dogma of molecular biology. Here, we present two spatial multi-omics technologies for spatially resolved genome-wide joint mapping of epigenome and transcriptome by co-profiling chromatin accessibility and gene expression (spatial-ATAC-RNA-seq) or histone modification and gene expression (spatial-CUT&Tag-RNA-seq) on the same tissue section at a resolution near single cells. They were applied to embryonic and neonatal mouse brain as well as adult human brain to map how epigenetic states or modifications regulate cell type and dynamics in tissue. Although distinct tissue features were identified by either spatial epigenome or spatial transcriptome alone with high concordance, we observed their differential roles in defining cell states. In general, epigenetic state proceeds the development of transcriptional phenotype in relation to epigenetic lineage priming. We also observed high expression canonical markers such as PROX1 in the granular cell layer of the human hippocampus showed low chromatin accessibility that corresponded to a low level of RNA turnover rate, highlighting a divergent need for open chromatin or transcription to control cell identity and dynamics. Spatial epigenome-transcriptome co-profiling is a highly informative tool to study the mechanism of gene expression regulation in tissue and may enable a wide range of applications in life science and biomedical research.

Main Text

Single-cell multi-omics technologies offered the direct means to determine the relation between different layers of gene regulation[1-4]. However, spatial information in the tissue context, which is critical to understanding cellular function, is missing in single cell data. Furthermore, tissue dissociation leads to perturbation in cell state or introduces technical noise. Recently, spatial epigenomics, transcriptomics, and proteomics emerged to address this challenge[5,6]. Currently, most spatial technologies can capture only one layer of genomics information. Although it is possible to computationally integrate the data from multiple modalities[7], the mechanistic link between different layers of omics can not be readily uncovered. Thus, it is highly desirable to realize joint profiling of multiple omics. Previously, we developed DBiT-seq for spatially resolved co-measurement of transcriptomics and a panel of proteins to link select proteins to genome-wide gene expression. To further investigate the epigenetic mechanisms underlying gene expression regulation, we aim to develop joint profiling of epigenome and transcriptome pixel by pixel in tissue. Herein, we present two of such technologies for spatially resolved genome-wide co-mapping of epigenome and transcriptome by simultaneously profiling chromatin accessibility and gene expression (spatial-ATAC-RNA-seq) or histone modification and gene expression (spatial-CUT&Tag-RNA-seq) on the same tissue section at cellular level via a microfluidic deterministic co-barcoding strategy to implement the chemistries for spatial ATAC-seq[8] or CUT&Tag[6] and spatial transcriptome. We applied them to the mapping of embryonic and neonatal mouse brain as well as adult human brain hippocampus

to dissect epigenetic states or modifications in regulating cell type and dynamics in tissue. In general, distinct tissue features could be identified by either spatial epigenome or spatial transcriptome alone with high concordance, they do have differential roles in defining cell states. This work presents a versatile technology for spatial co-profiling of epigenome and transcriptome pixel by pixel in tissue at cellular level for identifying the mechanistic link between epigenetic state (chromatin accessibility or histone modification) and transcriptional phenotype directly in the tissue context. It opens new frontiers in spatial omics and may bring unprecedented opportunities to biological and biomedical research.

Technology design, workflow, and data quality

Spatial-ATAC-RNA-seq was realized by deterministic barcoding of transposase-accessible chromatin and transcriptome on the same tissue section[5] as shown in **Fig. 1a** and **Fig. S1**. It started with a fresh frozen tissue section fixed with formaldehyde and then processed with the DNA adapter loaded Tn5 transposition complex. This adapter sequence containing a universal ligation linker was then inserted into the transposase accessible genomic DNA loci. Subsequently, a biotinylated DNA adapter containing a poly-T sequence and a universal ligation linker was added to the tissue surface to bind to mRNAs followed by reverse transcription (RT) in tissue. Next, we placed a microfluidic chip on the tissue section to introduce a set of spatial barcodes Ai (i = 1-50/100), each flowing through a different microchannel and then covalently linked to the DNA adapters through the universal ligation linker via templated ligation. Then, this microfluidic chip was replaced by another one that has microchannels perpendicular to the first flow direction to introduce another set of spatial barcodes Bj (j = 1-50/100) that were ligated to barcodes Ai (j = 1-50/100) using a similar ligation chemistry, resulting in a 2D grid of spatially barcoded tissue pixels, each of which had a unique combination of barcodes Ai and Bj (i = 1-50/100, j = 1-50/100, n of barcoded pixels = 2,500/10,000). Finally, barcoded cDNA and genomic DNA (gDNA) fragments were collected by reserve crosslinking. cDNAs were enriched with streptavidin beads and gDNA fragments were retained in the supernatant. Afterwards, gDNA and cDNA libraries were constructed separately during PCR amplification. We also developed spatial-CUT&Tag-RNA-seq for spatially resolved co-sequencing of histone modification and transcriptome on the same tissue section at cellular level. Similarly, this was implemented by conducting co-assay of cleavage under targets and tagmentation (CUT&Tag) and transcriptome on the same tissue area with the aforementioned microfluidic deterministic barcoding strategy[5], as depicted in **Fig. 1b** and **Fig. S2**. First, the antibody against the target histone modification was incubated with the paraformaldehyde fixed tissue section on a glass slide. Then, a secondary antibody was added to improve the tethering of transposome (pA-Tn5). After transposome activation, the DNA adapter with the universal ligation linker was inserted into the histone mark-specific genomic DNA loci. The subsequent steps were similar to spatial-ATAC-RNA-seq for constructing gDNA and cDNA libraries for next generation sequencing.

We performed spatial-ATAC-RNA-seq experiments on an embryonic day 13 mouse embryo (E13) and human hippocampus (Fig. 1c, 50 μm pixel size). For the ATAC portion in spatial-ATAC-RNA-seq, we obtained a median of 17,960 (E13) and 9,898 (hippocampus) unique fragments per pixel, of which 16% (E13) and 15% (hippocampus) of fragments overlapped with TSS regions, and 11% (E13) and 11%

(hippocampus) were located in peaks. The proportion of mitochondrial fragments is 1% for E13 and 20% for human hippocampus. For the RNA portion of spatial-ATAC-RNA-seq, the UMIs per pixel and detected genes were found to be an average of 1,038 genes (E13) and 1,200 genes (hippocampus) per pixel (**Fig. 1d**) and the total number of genes detected was 19,887 (E13) or 29,293 (hippocampus). We performed both spatial-ATAC-RNA-seq and spatial-CUT&Tag-RNA-seq experiments on mouse postnatal day 21 (P21) brain (Fig. 1c, 20 µm pixel size). For the ATAC (spatial-ATAC-RNA-seq) or CUT&Tag (spatial-CUT&Tag-RNA-seq) data, we obtained a median of 10,857 (ATAC) and 4,756 (CUT&Tag) unique fragments per pixel, of which 20% (ATAC) and 19% (CUT&Tag) of fragments overlapped with TSS regions, 24% (ATAC) and 19% (spatial-CUT&Tag-RNA-seq) located in peaks. The proportion of mitochondrial fragments was 0.1% for spatial-CUT&Tag-RNA-seq and 9% for spatial-ATAC-RNA-seq. For the RNA potion of spatial-ATAC-RNA-seq and spatial-CUT&Tag-RNA-seq, totally 19,859 genes (spatial-ATAC-RNA-seq) or 19,831 genes (spatial-CUT&Tag-RNA-seq) were detected with an average of 1,005 genes (spatial-ATAC-RNA-seq) and 1,145 genes (spatial-CUT&Tag-RNA-seq) per pixel (**Fig. 1d**) in the mouse brain tissues.

To further increase the mapping area, we also developed a new device to perform in tissue barcoding of 100x100 pixels and demonstrated it for spatial-ATAC-RNA-seq on an E13 mouse embryo sample (**Fig. 1c**, 25 µm pixel size). For the ATAC portion of the data, we obtained a median of 15,633 unique fragments per pixel, of which 15% of fragments overlapped with TSS regions, and 13% were in peaks. The proportion of mitochondrial fragments was 0.5%. For the RNA portion of the data, it detected 21,478 genes in total with an average of 550 genes per pixel (**Fig. 1d**) due to a lower sequencing depth. Moreover, the insert size distributions of chromatin accessibility (spatial-ATAC-RNA-seq) and histone modification (spatial-CUT&Tag-RNA-seq) fragments were consistent with the captured nucleosomal fragments in all tissues (**Fig. 1e** and **Fig. S3a-c**).

Mouse embryo: spatial co-mapping of chromatin accessibility and transcriptome to identify tissue feature, cell state and developmental dynamics

Spatial-ATAC-RNA-seq of a E13 mouse embryo identified eight major clusters using ATAC data and 15 clusters using RNA data. The distinct patterns of these clusters on the spatial map are in agreement with the tissue histology (see H&E staining of an adjacent tissue section, **Fig. 2a** and **Fig. S5a**). In the ATAC data, cluster 2 represents the eye in the mouse embryo with open chromatin accessibility for *Six6* (**Fig. 2d**). Cluster 3 to 5 are associated with several developing internal organs. Cluster 6 to cluster 7 cover the peripheral and central nervous system (PNS and CNS). In order to benchmark the ATAC data, we projected the ENCODE reference ATAC-seq from different embryonic organs onto our ATAC UMAP embedding. In general, the clusters are in good concordance with the ENCODE ATAC-seq projection (**Fig. S4a-d**). Cell type-specific marker genes were identified for individual clusters and their expressions were inferred from chromatin accessibility (**Fig. 2d-e** and **Fig. S5b-d**). *Sox2,* which is involved in the development of nervous tissue especially for the optic nerve formation, showed high chromatin accessibility in the embryonic eye field but also the ventricular layer with enriched neural stem/progenitor cells. *Myt1l*, which encodes myelin transcription factor 1 like protein, was activated in the embryonic brain and neural tube. *Nrxn2,* which encodes Neurexin 2, a key gene in the vertebrate nervous system, was observed extensively

in most neural cells. *Six6*, a key gene involved in eye development, showed highest activity and expression in the embryonic eye region. *Rbfox3*, a slicing factor well known as the nuclear biomarker NeuN, was observed extensively in all neural cells while *Sox1* appeared to be enriched in the ventricular layer (**Fig. S5**). Cell type-specific enrichment of transcription factor (TF) regulators were also examined using deviations of TF motifs (**Fig. S6**). We observed that *Sox2* transcription factor was enriched in cluster 8, consistent with its function in the embryonic brain development. *Nfib* motif was also enriched in the embryonic brain, which is necessary for proper brain development (**Fig. S6a**). The GREAT analysis further verified the strong concordance between gene regulatory pathways and anatomical annotation (**Fig. S6c**). We integrated spatial ATAC data with scRNA-seq data for cell type assignment in each cluster[9] (**Fig. 2b** and **Fig. S5e**). For instance, radial glia (neural stem/progenitor cells) were observed predominantly in the ventricular layer and the differentiated cell types such as granule neurons and inhibitory interneurons were enriched in distinct regions of the embryonic brain (**Fig. S5e-f**). For the RNA data, 15 distinct clusters were identified and characterized by specific marker genes (**Fig. 2a** and **Fig. S6d**). Their spatial patterns also agreed with the tissue histology shown in the H&E staining from an adjacent tissue section (**Fig. 2a** and **Fig. S5a**). For example, cluster 11 correlated with the embryonic eye, and also has the same maker *Six6* as identified in ATAC data (**Fig. 2d**). Clusters 2, 5, 7, 9, and 10 are related to PNS and CNS. Cluster 8 is associated with limb and bone development (**Fig. 2d** and **Fig. S5b-d**). The pathway analysis[10] results are consistent with anatomical annotation (**Fig. S7**).

What is unique in this work is co-profiling of epigenome and transcriptome, which allows for investigating the correlation between accessibility peaks and expressed genes pixel by pixel and predicting the interactions between different regulatory regions. Some enhancers (*Sox2*, *Mytl1*, *Sox1*, *Rbfox3,* and *Nrxn2*) were found to have dynamically regulated promoter interactions (**Fig. 2e**). For example, enhancers for *Sox2* and *Mytl1*, had higher chromatin accessibility specially in cluster 6 and 7, suggesting their roles in these regions to regulate *Sox2* and *Mytl1* expression. Moreover, we found that the some of the marker genes identified from ATAC data were enriched in part of the embryonic brain (for example, *Nrxn2*, and *Myt1l*) but not highly expressed in RNA data (**Fig. 2d** and **Fig. S5b**), which may indicate the lineage priming of these genes in embryonic brain[7]. The discordance between chromatin accessibility and gene expression proves the importance of spatial multi-omics co-profiling, which can help decipher the epigenetic mechanisms regulating gene expression. The integration of the RNA data with the scRNA-seq data[9] was also performed to assign the cell identities to each cluster (**Fig. 2b** and **Fig. S5f**). We observed that the radial glia, granule neurons, and inhibitory interneurons were present in the same major clusters as shown in the ATAC analysis, which verified the power to define cell identities from multiple omics information. It was also attempted to use joint clustering of the ATAC and RNA data to refine the spatial patterns. For example, we identified cluster 11 (granule cells) in the joint clustering analysis, which was not readily resolved by single modalities alone (**Fig. 2a**, right). This result highlights the unique value to use joint multi-omics profiles for improving the cell-type-specific spatial mapping[11].

To investigate the dynamic relationship between chromatin accessibility and gene expression during embryonic development, we analyzed the differentiation trajectory from radial glia cells to various types

of neurons[12] such as inhibitory interneurons. The pseudotime analysis[13] was conducted on both ATAC and RNA data in spatial-ATAC-RNA-seq, and the results identified interneuron heterogeneity and the developmental trajectories, which were directly visualized in the spatial tissue map (**Fig. 2f, g**). The gene activity scores for chromatin accessibility and gene expression along this developmental trajectory were computed and the dynamic changes in select marker genes were presented (**Fig. 2h, i**). Overall, the gene expression exhibited a similar temporal tendency as the chromatin accessibility, but showed a slower pace during the developmental process, such as *Sox11* and *Nfix*, in agreement with epigenetic lineage-priming of gene expression[7]. Thus, our spatial-ATAC-RNA-seq can be used to decipher the gene regulation mechanism and dynamics during tissue development.

Postnatal mouse brain: spatial co-mapping of chromatin accessibility or chromatin modification with transcriptome at the cellular level

We conducted spatial mapping of P21 mouse brain coronal sections (at Bregma 1) for both chromatin accessibility and histone modification jointly with transcriptome. Either ATAC or RNA data identified 9 clusters with distinct spatial distribution in agreement with anatomical annotation defined by the Nissl staining (**Fig. 3a** and **Fig. S10a**). Spatial clusters between ATAC and RNA showed strong concordance in cluster assignment (**Fig. S15b**). For ATAC data, unique chromatin accessibility resolved clusters within specific regions. For example, medium spiny neurons (*Pde10a,* cluster 1), corpus callosum (*Sox10, Mobp,* and *Tspan,* cluster 3), and the ventricular zone (*Notch1,* cluster 7) (**Fig. 3c** and **Fig. S8a**). Cell type-specific chromatin regulatory elements were analyzed (**Fig. S11**) that may act as cell type-specific reporters. The GREAT analysis confirmed that the pathways correlated with the tissue functions in different anatomical regions (**Fig. S11b**). For the RNA data, the clusters also showed specific gene expression within individual regions. For example, medium spiny neurons (*Pde10a,* cluster 1), and corpus callosum (*Mobp,* and *Tspan2,* cluster 4) (**Fig. 3c** and **Fig. S8b**).

Integration of single-cell ATAC-seq of the mouse brain atlas data[14] with our spatial ATAC data was carried out (**Fig. 3d**) to identify all major cell types[15] and then used the label transfer to assign cell types to spatial locations where epigenetic state may control specific cell type formation (**Fig. S10b**). For example, an enrichment of mature oligodendrocytes (MOLs) was observed within corpus callosum. A thin layer of ependymal cells (EPENs) was identified in the ventricular zone, and medium spiny neurons (MSNs) were found to be enriched in striatum (**Fig. S10b**). We then integrated our spatial RNA data with scRNA-seq[15] and again used label transfer to identify the dominant cell types in each cluster (**Fig. 3e, j** and **Fig. S10b**). We observed a high degree of concordance in cell type identification between integrated ATAC and integrated RNA data analyses, suggesting a general congruence between chromatin accessibility and transcriptome to define cell identities in tissue. For example, the ependymal cells (EPEN), medium spiny neuron (MSN), and mature oligodendrocytes (MOL) revealed by the RNA data were enriched in the same regions as identified by the ATAC data in spatial-ATAC-RNA-seq (**Fig. S10b**). Furthermore, the detection of a thin layer of EPEN cells in the ventricular zone demonstrated a high spatial resolution for our

technology to identify low abundance cells at near-single cell resolution. The result was further improved by joint clustering of ATAC and RNA profiles (**Fig. 3a**, bottom).

Joint profiling of ATAC and RNA allows for searching the correlated peak accessibility and gene expression to predict putative enhancers. We detected 21,791 significant peak-to-gene linkages between regulatory elements and target genes (**Fig. S10d** and **Fig. S15a**). Some potential enhancers with dynamically regulated promoter interactions were found to be cluster-specifically enriched, such as *Sox10* (cluster 3, and cluster 8), *Notch1* (cluster 3, cluster 6, cluster 7, and cluster 8), *Tspan2* (cluster 3), and *Mobp* (cluster 3) (**Fig. 3k** and **Fig. S8c**), indicating the ability for spatial-ATAC-RNA-seq to identify the key regulatory regions. The annotation of cell type-specific chromatin regulatory elements and TF regulators (*Sox10, Atoh7, Nifx, Nfic,* and *Neurod6*) in relation to the spatial pattern provided further insights to the regulatory factors in the tissue context (**Fig. S11a** and **Fig. S12**). For example, *Sox10* was examined for chromatin accessibility, gene expression, putative enhancers, and TF activities simultaneously, permitting more comprehensive understanding of gene regulation dynamics. We found that some highly active marker genes with open chromatin accessibility (i.e., *Notch1*) were not highly expressed for transcription (**Fig. 3c**), suggesting the possibility of linage-priming of these genes in the brain tissue development[7].

In addition to chromatin accessibility, histone modifications are also important aspects in epigenetic regulation. Spatial-CUT&Tag-RNA-seq was performed to profile transcriptome and H3K27ac (activating enhancers and/or promoters) in P21 mouse brain with 20 μm pixel size, which identified 7 and 9 specific clusters for CUT&Tag and RNA, respectively (**Fig. 3b**). Overall, these clusters agreed with the anatomical regions defined by the Nissl staining from an adjacent tissue section (**Fig. 3b** and **Fig. S10a**) and also good concordance between CUT&Tag and RNA in terms of spatial patterns (**Fig. S16b**). For the CUT&Tag data, the cluster specific active genes were shown in gene activity score (GAS) (**Fig. 3c** and **Fig. S9a**). For example, *Sox10, Mal,* and *Cldn11* showed high gene activity score in cluster 3 (corpus callosum), *Notch1* activity enriched in cluster 2 (the ventricular zone), and *Pde10a* highly active in cluster 4 (medium spiny neuron). We also identified TF motifs in H3K27ac modification loci, which could help better understand the most active regulatory factors across all clusters (**Fig. S13a** and **Fig. S14**) and the pathway enrichment by GREAT agreed with the tissue function in different anatomical regions (**Fig. S13b**). The RNA data clusters showed unique signature within specific marker gene regions (**Fig. 3c** and **Fig. S9b**) as exemplified by medium spiny neurons (*Pde10a,* cluster 4) and corpus callosum (*Sox10, Cldn1,* and *Mal,* cluster 2) (**Fig. 3c**).

Integration of our CUT&Tag data with the scCUT&Tag data[16] (**Fig. 3f, i**) also allowed for label transfer[15] to assign epigenetic cell identities/states to spatial location (**Fig. S10c**). We also observed an enrichment of MOL1 within the corpus callosum, a thin layer of EPEN in ventricular zone, and MSN1 in the striatum, in agreement with spatial-ATAC-RNA-seq data (**Fig. S10c**), suggesting the important role for H3K27ac to control the development of all major tissue types in this brain region. We also integrated the RNA part of the spatial-CUT&Tag-RNA-seq data with scRNA-seq[15] to identify dominant cell types in each cluster via label transfer (**Fig. 3g, j** and **Fig. S10c**). MOL1, a thin layer of EPEN, and MSN1 were enriched in the same

spatial regions recognized by CUT&Tag (**Fig. S10c**). Joint clustering of CUT&Tag and RNA could further enhance the resolution of spatial clusters (**Fig. 3b**)[11]. To directly interrogate the interactions between specific gene expression and the corresponding enhancers across all clusters, we identified a total of 16,973 significant peak-to-gene linkages (**Fig. S16a**) such as *Sox10* (cluster 3), *Notch1* (cluster 2, cluster 3, cluster 5, and cluster 6), *Mal* (cluster 3), and *Cldn11* (cluster 3) (**Fig. 3l** and **Fig. S9c**). We also found that some of the highly activated marker genes identified by CUT&Tag (i.e., *Notch1*) were not highly expressed (**Fig. 3c**), which may also suggest the lineage-priming[7], in this case, mediated by H3K27ac.

Human brain hippocampus: co-mapping of accessible chromatin and transcriptome to dissect cell type, dynamics, and gene regulation

We performed spatially resolved co-sequencing of epigenome and transcriptome (50 μm pixel size) on adult human brain hippocampal formation, which is a highly complex brain region involved in high level cognitive function and neurological diseases such as major depression disease (MDD) and Alzheimer's disease (AD). Neuronal cell types, fate, and dynamics in this region remains poorly understood. We identified 7 and 8 major clusters for ATAC and RNA, respectively, and the spatial distribution corresponds well to the major anatomical regions by the Nissl staining (**Fig.4a**). For the ATAC data, cluster 4 is the granular cell layer (GCL) (*THY1*, *BCL11B*) and cluster 6 is the choroid plexus (**Fig. 4a, d**). The TF motifs (*ID4,* and *MESP1*) and their spatial patterns were analyzed to identify the regulatory factors in different tissue regions (**Fig. S17b**). For the RNA data, we also detected distinct clusters with unique marker genes (**Fig. 4a, d**) such as *PROX1* and *BCL11B* enriched in cluster 4 (GCL).

To directly interrogate the gene regulatory interactions between regulated promoters and specific enhancers, the correlation of peak accessibility and gene expression was analyzed (**Fig. 4e**) and identified some enhancers with dynamically regulated promoter interactions, such as *SOX2* (cluster 0, cluster1, and cluster 3). This also suggests that spatial-ATAC-RNA-seq allows for mapping chromatin accessibility dynamics at different regulatory regions directly in the spatial tissue context such as the human hippocampus.

We also conducted data integration with single-cell ATAC or RNA sequencing. Combining the ATAC part of our data with scATAC-seq[17] revealed the dominant cell identities in individual clusters (**Fig. 4b**). In addition, the RNA part of our data was integrated with scRNA-seq data[18] to assign transcriptional cell types to each cluster via label transfer (**Fig. 4c** and **Fig. S17a**). The granule cells were detected clearly in the GCL, the cornu ammonis (CA) neurons were enriched in CA3-4 regions, and the vascular and leptomeningeal cells (VLMC) were strongly distinguished in choroid plexus (ChPx) as opposed to other regions.

In general, both ATAC and RNA can readily resolve all major tissue features in this region but spatial co-sequencing of epigenome and transcriptome can provide new insights into the dynamic gene regulation mechanism which cannot be realized by single modalities. For example, *PROX1,* a signature gene defining the granule neuron identity during pyramidal neuron fate selection[19], is indeed highly expressed

in GCL but showed low chromatin accessibility (**Fig. 4d**). This could be attributed to a minimal demand to synthesize new *PROX1* transcripts in postmitotic mature granule neurons and thus not needed to maintain an active open chromatin state for *PROX1*.

To verify this hypothesis, we conducted RNA velocity analysis to examine cell dynamics by quantifying tissue region specific RNA turnover rate (**Fig. 4f**). Overall, the RNA velocity map identified the major branches corresponding to, for example, GCL of the dentate gyrus (DG) and CA region, which is consistent with the neuronal developmental lineage relationship as well as the anatomical and functional subdivisions of hippocampus[19]. Using RNA velocity to examine the dynamics of selected genes (**Fig. 4g**) confirmed that *PROX1* has a low RNA turnover rate despite highest expression level in GCL. Together with the discordance between chromatin accessibility and gene expression (**Fig. 4d**), these results suggested that *PROX1* activity is differentially required in regions during adult human brain hippocampus in agreement with the findings in murine studies[20]. *PLP1*, which plays an important role in oligodendrocyte development and myelin sheath maintenance, showed high expression in oligodendrocytes enriched white matter region but relatively low chromatin accessibility, which also correlated with a low level of RNA turnover (**Fig. 4g**). *BCAS1*, a key gene required for myelination, had high chromatin accessibility in the white matter region but the gene expression was low, which corresponded to a high level of RNA turnover despite low gene expression (**Fig. 4g**). Cell dynamics revealed by RNA velocity for *PROX1*, *PLP1*, and *BCAS1* validated our findings from the discordance between chromatin accessibility and gene expression. In general, high RNA velocity is associated with more accessible chromatin while low RNA turnover was detected in closed chromatin. These results further highlighted the importance of spatial multi-omics mapping to fully dissect not only cell state but also developmental dynamics in a highly heterogeneous tissue.

Discussion

We developed spatial-ATAC-RNA-seq and spatial-CUT&Tag-RNA-seq for co-profiling of genome-wide chromatin accessibility or histone modification in conjunction with whole transcriptome on the same tissue section with near single cell resolution (20 μm pixel size). Spatial-ATAC-RNA-seq was applied to E13 mouse embryo to reveal the tissue-type-specific epigenetic regulations and gene expression, which provided two layers of spatial information at tissue scale with data quality as good as previously obtained by single modalities. Spatial-temporal changes between chromatin accessibility and gene expression during development were explored. Spatial-ATAC-RNA-seq and spatial-CUT&Tag-RNA-seq on mouse brain demonstrated the ability to directly interrogate the relationship between epigenome and transcriptome at cellular level in a spatially resolved manner, enabling the definition of cell identities from two aspects and identification of cells and genes regulated by epigenetic lineage priming. Applying spatial-ATAC-RNA-seq to human hippocampus resolved distinct subregions and corresponding cell types. Co-profiling of epigenomic and transcriptomic more precisely delineated cell state and dynamics. Interestingly, we observed the discordance between epigenetic and transcriptional state, which was

attributed to their differential role in producing or maintaining gene expression. RNA velocity that can reveal cell dynamics by quantifying RNA turnover rate further confirmed our findings.

While most data were collected using a design for mapping 50x50 pixels, we also demonstrated a 4x larger mapping area in an E13 mouse embryo for co-profiling ATAC and RNA using 100 x100 barcodes (total 10,000 pixels, 25 µm pixel size) (**Fig. S18**). It is possible to further increase the mapping area by increasing the number of barcodes and implement the microfluidic barcoding process in an automated liquid handling system to increase throughput.

We have demonstrated either ATAC or CUT&Tag in conjunction with RNA for spatial multi-omics mapping, it is possible to further combine all three – chromatin accessibility, histone modifications, and transcriptome – to delineate a more comprehensive landscape of gene regulation network in tissue. It is also desirable to measure multiple histone modifications to assess the multivalency effect on gene expression regulation in different tissue regions. Previously, we have demonstrated spatial profiling of transcriptome and a panel of proteins. We envision it is possible and highly valuable to further combine epigenome, transcriptome, and proteome[21] to provide a tri-omics landscape of cell type, state, and gene regulation. Finally, we envision spatial multi-omics as reported herein may find more important applications in human disease research and the data from multi-modalities can not only cross-validate one another but better elucidate the mechanisms driving abnormal cell states that could have been difficult to discern using single modality methods. In addition, the spatial mapping may further reveal how the local tissue environment affects cell state, dynamics, and function.

In summary, spatially resolved genome-wide co-sequencing of epigenome and transcriptome at the cellular level represents one of the most informative tools in spatial biology and well positioned to be adopted in a wide range of biological and biomedical research.

Methods

Preparation of tissue slides

Mouse C57 Embryo Sagittal Frozen Sections (MF-104-11-C57) was purchased from Zyagen (San Diego, CA).

The mouse brain tissue sections were got from Karolinska Institutet. The mouse line used is Sox10:Cre-RCE:LoxP (EGFP), on a C57BL/6xCD1 mixed genetic background. Experimental procedures on juvenile (P21) mice were conducted in accordance with the European directive 2010/63/EU, local Swedish directive L150/SJVFS/2019:9, Saknr L150, and Karolinska Institutet complementary guidelines for procurement and use of laboratory animals, Dnr 1937/03-640. All the procedures were approved by Stockholms Norra Djurförsöksetiska nämnd, the local committee for ethical experiments on laboratory animals in Sweden, lic.nr. 1995/2019.

The human brain tissue sections were obtained from the Brain Collection of the New York State Psychiatric Institute (NYSPI) and Columbia University. The brain sample was collected in the Republic of Macedonia of brain collection and autopsy was conducted with Institutional Review Board approvals and informed consent from the next of kin.

All the tissues were sectioned with a thickness of 10 μm and put on glass slides (63478-AS, Electron Microscopy Sciences). The samples were stored at -80 °C for further use.

Preparation of transposome

Unloaded Tn5 transposase (C01070010) and pA-Tn5 (C01070002) were purchased from Diagenode, and the transposome was assembled following manufacturer's guidelines. The oligos used for transposome assembly were as follows:

Tn5MErev:

 5'-/5Phos/CTGTCTCTTATACACATCT-3'

 Tn5ME-A:

 5'-TCGTCGGCAGCGTCAGATGTGTATAAGAGACAG-3'

 Tn5ME-B:

5'-/5Phos/CATCGGCGTACGACTAGATGTGTATAAGAGACAG-3'

DNA oligos, DNA barcodes sequences, and other key reagents

DNA oligos used for PCR and library construction were shown in Table S1, All the DNA barcodes sequences were given in Table S2 and S3, and all other chemicals and reagents were listed in Table S4.

Spatial-ATAC-RNA-seq:

The frozen tissue slide was thawed for 10 min at room temperature. The tissue was fixed with formaldehyde (0.2%, with 0.05 U/μL RNase Inhibitor) for 5 min and quenched with 1.25 M glycine for another 5 min. After fixation, the tissue was washed with 1 mL 0.5X DPBS-RI twice and cleaned with DI water.

The tissue permeabilization was done with 200 μL lysis buffer (3 mM $MgCl_2$; 0.01% Tween-20; 10 mM Tris-HCl, pH 7.4; 0.01% NP-40; 10 mM NaCl; 1% BSA; 0.001% Digitonin; 0.05 U/μL RNase Inhibitor) for 15 min and was washed by 200 μL wash buffer (10 mM Tris-HCl pH 7.4; 10 mM NaCl; 3 mM $MgCl_2$; 1% BSA; 0.1% Tween-20) twice for 5 min. Transposition mix (5 μL home-made transposome; 33 μL 1X DPBS; 50 μL 2X Tagmentation buffer; 1 μL 1% Digitonin; 1 μL 10% Tween-20; 0.05 U/μL RNase Inhibitor; 10 μL Nuclease-free H_2O) was added and incubated at 37 °C for 30 min. After that, 200 μL 40 mM EDTA with

0.05 U/µL RNase Inhibitor was added and incubated for 5 min at room temperature to stop transposition. Finally, the tissue section was washed with 200 µL 0.5X PBS-RI twice for 5 min and cleaned with DI water.

For reverse transcription, RT mixture (12.5 µL 5X RT Buffer; 4.5 µL RNase-free water; 0.4 µL RNase Inhibitor; 0.8 µL SuperaseIn RNase Inhibitor; 3.1 µL 10 mM dNTPs each; 6.2 µL Maxima H Minus Reverse Transcriptase; 25 µL 0.5X PBS-RI; 10 µL RT primer) was added. The tissue was incubated 30 min at room temperature, and 42°C for 90 min in a wet box. After RT reaction, the tissue was washed with 1X NEB buffer 3.1 with 1% RNase Inhibitor for 5min.

For 1st barcode (barcode A) *in situ* ligation, the 1st PDMS chip was covered to the region of interest (ROI) on the tissue. For alignment purpose, 10X objective (Thermo Fisher EVOS fl microscope) was used to take a brightfield image. The PDMS device and tissue slide were clamped with a home-made acrylic clamp tightly. At first, barcode A was annealed with ligation linker 1, 10 µL 100 µM ligation linker, 10 µL 100 µM each barcode A, and 20 µL 2X annealing buffer (20 mM Tris; pH 7.5-8.0; 100 mM NaCl; 2 mM EDTA) were mixed well. For each channel, 5 µL ligation master mixture was prepared with 2 µL of ligation mix (27 µL of T4 DNA ligase buffer; 72.4 µL of RNase free water; 5.4 µL of 5% Triton X-100; 11 µL T4 DNA ligase), 2 µL of 1X NEBuffer 3.1, and 1 µL of each annealed DNA barcode A (A1-A50/A100, 25 µM). Vacuum was used to load ligation master mixture into 50 channels of the device. The device was incubated at 37 °C for 30 min in a wet box. The PDMS chip and clamp were removed after washed with 1X NEBuffer 3.1 for 5 min. The slide was washed with water and dried by air.

For 2nd barcode (barcodes B) *in situ* ligation, the 2nd PDMS chip was covered to the slide. Another brightfield image with 10X objective was taken. The acrylic clamp was applied to clamp the PDMS and tissue slide together. The annealing of barcodes B (B1-B50/B100, 25 µM) and the preparation of ligation master mix were the same with barcodes A. The device was incubated at 37 °C for 30 min in a wet box. The PDMS chip and clamp were removed after washed with 1X DPBS with SUPERase In RNase Inhibitor for 5 min. The slide was washed with water and dried by air. The brightfield image was taken for further alignment.

For lysis of the tissue, the ROI of the tissue was digested with 100 µL reverse crosslinking mixture (0.4 mg/mL proteinase K; 1 mM EDTA; 50 mM Tris-HCl, pH 8.0; 200 mM NaCl; 1% SDS) at 58 °C for 2 h in a wet box. The lysate was collected into a 1.5 mL tube and incubated at 65 °C overnight.

For DNA and cDNA separation, the lysate was purified with Zymo DNA Clean & Concentrator-5 and eluted to 100 µL of RNase free water. The 1X B&W buffer with 0.05% Tween- 20 was used to wash 40 µL Dynabeads MyOne Streptavidin C1 beads for 3 times. Then 200 µL 2X B&W buffer with 2.5 µL of SUPERase In RNase Inhibitor was used to resuspend the beads. The resuspended beads were mixed with the lysate and allowed binding at room temperature for 1 h with agitation. A magnet was used to separate beads and supernatant in the lysate.

The supernatant was taken out for ATAC library construction. The supernatant was purified with Zymo DNA Clean & Concentrator-5 and eluted to 20 µL of RNase free water. PCR solution (25 µL 2X NEBNext

Master Mix; 2.5 µL 25 µM N7XX primer; 2.5 µL 25 µM P5 PCR primer) was added and mix well. The PCR was first conducted by following the program: 72°C 5 min, 98°C 30 s, and cycled at 98°C 10 s, 63°C 10 s, and 72°C 1 min for 5 times. To figure out additional cycles, the pre-amplified mixture (5 µL) was mixed with qPCR solution (5 µL 2X NEBNext Master Mix; 0.24 µL 25X SYBR Green; 0.5 µL 25 µM new P5 PCR primer; 3.76 µL nuclease-free H$_2$O; 0.5 µL 25 µM N70X primer). Then, qPCR reaction was conducted as following program: 98 °C 30 s, and cycled at 98 °C 10 s, 63 °C 10 s, and 72°C 1 min for 20 times. The remaining pre-amplified DNA (45 µL) was amplified by running additional cycles determined by qPCR (reach 1/3 of saturated signal). The final PCR product was purified by 1X Ampure XP beads (45 µL) and eluted in 20 µL nuclease-free H$_2$O.

The beads were used for cDNA library construction. The beads were washed twice with 400 µL 1X B&W buffer with 0.05% Tween-20 and once more with 10mM Tris (pH 8.0) containing 0.1% Tween-20. Streptavidin beads with bound cDNA molecules were resuspended in a TSO solution (22 µL 10 mM dNTPs each; 44 µL 5X Maxima RT buffer; 44 µL 20 % Ficoll PM-400 solution; 88 µL RNase free water; 5.5 µL of 100uM template switch primer; 11 µL of Maxima H Minus Reverse Transcriptase; 5.5 µL of RNase Inhibitor). The beads were incubated at room temperature for 30 min and then at 42°C for 90 min with gentle shaking. After washing beads once with 400 µL 10 mM Tris with 0.1% Tween-20 and once with water, the beads were resuspended into a PCR solution (110 µL 2X Kapa HiFi HotStart Master Mix; 8.8 µL 10 µM primer 1 and primer 2; 92.4 µL RNase free water). The
PCR thermocycling was performed as following program: 95°C 3 min, and
cycled at 98°C 20 s, 65°C 45 s, 72°C 3 min for 5 times.
After five cycles, Dynabeads MyOne Streptavidin C1 beads was removed from PCR solution and 25X SYBR Green was added at 1X concentration. Samples were again placed in a qPCR machine with the following thermocycling conditions: 95°C for 3 min, cycled at 98°C 20 s, 65°C 20 s, and 72°C 3 min for 15 times, followed by a single 5 minutes at 72°C after cycling. The reaction was removed once qPCR signal began to plateau. The PCR product was purified with a 0.8X Ampure XP beads and eluted in 20 µL nuclease-free H$_2$O.

A Nextera XT Library Prep Kit was used for library preparation. The purified cDNA (1 ng) was diluted in RNase free water to a total volume of 5 µL. 10 µL Tagment DNA buffer and 5 µL Amplicon Tagment mix was added and incubated at 55°C for 5 min. 5 µL of NT buffer was added and incubated at room temperature for 5 min. PCR master solution (15 µL PCR master mix; 1 µL 10 µM P5 primer; 1 µL 10 µM indexed P7 primer; 8 µL RNase free water) was added and PCR reaction was performed with the following program: 95°C 30 s, cycled at 95°C 10 s, 55°C 30 s, 72°C 30 s, and 72°C for 5 min after 12 cycles. The PCR product was purified with a 0.7X Ampure XP beads to get the library.

The Agilent Bioanalyzer High Sensitivity Chip was used to get the size distribution and concentration of the library before sequencing. Next Generation Sequencing (NGS) was conducted on Illumina NovaSeq 6000 sequencer (pair-end 150 bp mode).

Spatial-CUT&Tag-RNA-seq:

The frozen tissue slide was thawed for 10 min at room temperature. The tissue was fixed with formaldehyde (0.2%, with 0.05 U/µL RNase Inhibitor) for 5 min and quenched with 1.25M glycine for another 5 min. After fixation, the tissue was washed with 1 mL wash buffer (150 mM NaCl; 20 mM HEPES pH 7.5; 1 tablet Protease inhibitor cocktail; 0.5 mM Spermidine) twice and dip into DI water. The tissue section was permeabilized with NP40-Digitonin wash buffer (0.01% Digitonin; 0.01% NP40; in wash buffer) for 5 minutes. The primary antibody (Table S3) (1:50 dilution with antibody buffer (0.001% BSA; 2 mM EDTA; in NP40-Digitonin wash buffer) was added and incubated at 4 °C overnight. The secondary antibody (Table S3) (1:50 dilution with NP40-Digitonin wash buffer) was added and incubated 30 min at room temperature. The tissue was washed with wash buffer for 5 min. A 1:100 dilution of pA-Tn5 adapter complex in 300-wash buffer (1 tablet Protease inhibitor cocktail; 300 mM NaCl; 0.5 mM Spermidine; 20 mM HEPES pH 7.5) was added and incubated at room temperature for 1 h. Then followed with a 5 min wash with 300-wash buffer. Tagmentation buffer (10 mM $MgCl_2$ in 300-wash buffer) was added and incubated at 37 °C 1 h. Then, 40 mM EDTA with 0.05 U/µL RNase Inhibitor was added and incubated at room temperature for 5 min to stop tagmentation. The tissue was washed twice with 0.5X DPBS-RI for 5 min for further use.

For reverse transcription, two ligations, and beads separation, the protocols were the same with Spatial-ATAC-RNA-seq.

For the construction of CUT&Tag library, the supernatant was purified with Zymo DNA Clean & Concentrator-5 and eluted to 20 µL of RNase free water. PCR solution (2 µL 10 µM P5 PCR primer and indexed i7 primer; 25 µL NEBnext PCR Master Mix) was added and mixed well. The PCR was performed with the program: 58 °C 5 min, incubated at 72 °C 5 min and 98 °C 30 s, then cycled at 98 °C 10 s, and incubated at 60 °C 10 s for 12 times, and final incubated at 72 °C 1 min. The PCR product was purified by 1.3X Ampure XP beads using the standard protocol and eluted in 20 µL nuclease-free H_2O.

The cDNA libraries construction followed the former spatial-ATAC-RNA-seq protocol.

The Agilent Bioanalyzer High Sensitivity Chip was used to get the size distribution and concentration of the library before sequencing. Next Generation Sequencing (NGS) was conducted on Illumina NovaSeq 6000 sequencer (pair-end 150 bp mode).

Data preprocessing

For ATAC and CUT&Tag data, linker 1 and linker 2 were used to filter Read 2, and the sequences were converted to Cell Ranger ATAC format (10x Genomics). The genome sequences were in the newly formed Read 1, barcodes A and barcodes B were included in newly formed Read 2. Human reference (GRCh38) or mouse reference (mm10) were used to align the fastq files. The achieved BED like fragments were used to conduct downstream analysis. The fragments file includes fragments information on spatial locations (barcode A x barcode B) and genome.

For RNA data, the Read 2 was refined to extract the Barcode A, Barcode B, and UMI. ST pipeline v1.7.2[22] was used to map the processed read 1 against the mouse genome (GRCm38) and human genome (GRCh38), which created the gene matrix for downstream analysis. The gene expression matrix contains information of genes and spatial locations (barcode A x barcode B).

Data clustering and visualization

We first identified location of pixels on the tissue from the bright light image using MATLAB, read the ATAC, CUT&Tag, and RNA matrix into Signac v1.6[23].

For RNA data visualization, the feature was set to 3000 with "FindVariableFeatures" function. Then the data was normalized using "SCTransform" function. Normalized RNA data was clustered and RNA UMAP was built with the dimension set to 10, the cluster resolution set to 0.8, and the algorithm set to 3.

For ATAC/CUT&Tag data visualization, the min.cutoff was set to 10 with "FindTopFeatures" function. The data was normalized and dimensional reduced using Latent Semantic Indexing (LSI). Then the ATAC/CUT&Tag data was clustered and ATAC/CUT&Tag UMAP was built with dimension set to 2:20, the cluster resolution set to 0.6, and the algorithm set to 3.

For visualization of integrated ATAC/CUT&Tag and RNA data[24], the "FindMultiModalNeighbors" function was used. The reducton.list was set to ("pca", "lsi"), the dims.list was set to (1:10, 2:20), the modality.weight.name was set to RNA.weight. The UMAP was built with the cluster resolution set to 0.8, and the algorithm set to 3.

As for RNA spatial data visualization, the gene matrix got from RNA was loaded into Seurat v4.1[25] as a Seuratobject, the metadata of RNA got from Signac was read into the Seuratobject. All the spatial maps were then plotted with the "SpatialPlot" function.

As for ATAC/CUT&Tag spatial data visualization, the fragment file got from ATAC/CUT&Tag was read into ArchR[26] as an ArchRProject, the metadata of ATAC/CUT&Tag got from Signac was read into the ArchRProject. The data from ArchRProject was normalized and dimensional reduced using iterative Latent Semantic Indexing (LSI). The getMarkerFeatures and getMarkers functions in ArchR (testMethod = "Wilcoxon", cutOff = "FDR <= 0.05", groupBy = "seurat_cluster") was used to find the marker genes/regions for each cluster. To visualize the spatial data, results got from ArchR were imputed to Seurat V4.1 to map the data back to the tissue. The size of the pixels were scaled using the "pt.size.factor" parameter in the Seurat package for better visualization.

For peak-to-gene link, we inputted RNA Seuratobject using "addGeneIntegrationMatrix" function in ArchR, then the peak-to-gene link was drawn with "addPeak2GeneLinks" function.

Published data for data quality comparison and integrative analysis

Resource	Platform	Link
ENCODE ATAC-seq (E13.5 mouse embryo)	bulk	https://www.encodeproject.org/search/?type=Experiment&status=released&related_series.@type=OrganismDevelopmentSeries&replicates.library.biosample.organism.scientific_name=Mus+musculus&assay_title=ATAC-seq&life_stage_age=embryonic%2013.5%20days
Mouse organogenesis cell atlas (MOCA)	scRNA-seq	https://oncoscape.v3.sttrcancer.org/atlas.gs.washington.edu.mouse.rna/downloads
Atlas of gene regulatory elements in adult mouse cerebrum	scATAC-seq	http://catlas.org/mousebrain/#!/downloads
Atlas of the Adolescent Mouse Brain	scRNA-seq	http://mousebrain.org/adolescent/downloads.html
Human hippocampus	scRNA-seq	https://www.ncbi.nlm.nih.gov/geo/query/acc.cgi?acc=GSE186538
Human hippocampus	scATAC-seq	https://www.ncbi.nlm.nih.gov/geo/query/acc.cgi?acc=GSE147672

Reporting summary

Further information on research design is available in the Nature Research Reporting Summary linked to this paper.

Code availability

Code for sequencing data analysis is available on Github: https://github.com/di-0579/Spatial_epigenome-transcriptome_co-sequencing

Data availability

Raw and processed data reported in this paper are deposited in the Gene Expression Omnibus (GEO) with accession code GSE205055 (reviewer token: klyzwcmmlnwjxmt).

References

1   Chen, S., Lake, B. B. & Zhang, K. High-throughput sequencing of the transcriptome and chromatin accessibility in the same cell. *Nat Biotechnol* **37**, 1452-1457, doi:10.1038/s41587-019-0290-0 (2019).

2   Allaway, K. C. *et al.* Genetic and epigenetic coordination of cortical interneuron development. *Nature* **597**, 693-697, doi:10.1038/s41586-021-03933-1 (2021).

3   Trevino, A. E. *et al.* Chromatin and gene-regulatory dynamics of the developing human cerebral cortex at single-cell resolution. *Cell* **184**, 5053-5069 e5023, doi:10.1016/j.cell.2021.07.039 (2021).

4   Cao, J. *et al.* Joint profiling of chromatin accessibility and gene expression in thousands of single cells. *Science* **361**, 1380-1385, doi:doi:10.1126/science.aau0730 (2018).

5   Liu, Y. *et al.* High-Spatial-Resolution Multi-Omics Sequencing via Deterministic Barcoding in Tissue. *Cell* **183**, 1665-1681 e1618, doi:10.1016/j.cell.2020.10.026 (2020).

6   Deng, Y. *et al.* Spatial-CUT&Tag: Spatially resolved chromatin modification profiling at the cellular level. *Science* **375**, 681-686, doi:doi:10.1126/science.abg7216 (2022).

7   Ma, S. *et al.* Chromatin Potential Identified by Shared Single-Cell Profiling of RNA and Chromatin. *Cell* **183**, 1103-1116 e1120, doi:10.1016/j.cell.2020.09.056 (2020).

8   Deng, Y. *et al.* Spatial-ATAC-seq: spatially resolved chromatin accessibility profiling of tissues at genome scale and cellular level. *bioRxiv*, 2021.2006.2006.447244, doi:10.1101/2021.06.06.447244 (2021).

9   Cao, J. *et al.* The single-cell transcriptional landscape of mammalian organogenesis. *Nature* **566**, 496-502, doi:10.1038/s41586-019-0969-x (2019).

10   Wu, T. *et al.* clusterProfiler 4.0: A universal enrichment tool for interpreting omics data. *Innovation (N Y)* **2**, 100141, doi:10.1016/j.xinn.2021.100141 (2021).

11   Zhu, C. *et al.* Joint profiling of histone modifications and transcriptome in single cells from mouse brain. *Nat Methods* **18**, 283-292, doi:10.1038/s41592-021-01060-3 (2021).

12   Kriegstein, A. & Alvarez-Buylla, A. The Glial Nature of Embryonic and Adult Neural Stem Cells. *Annual Review of Neuroscience* **32**, 149-184, doi:10.1146/annurev.neuro.051508.135600 (2009).

13   Trapnell, C. *et al.* The dynamics and regulators of cell fate decisions are revealed by pseudotemporal ordering of single cells. *Nat Biotechnol* **32**, 381-386, doi:10.1038/nbt.2859 (2014).

14   Li, Y. E. *et al.* An atlas of gene regulatory elements in adult mouse cerebrum. *Nature* **598**, 129-136, doi:10.1038/s41586-021-03604-1 (2021).

15   Zeisel, A. *et al.* Molecular Architecture of the Mouse Nervous System. *Cell* **174**, 999-1014 e1022, doi:10.1016/j.cell.2018.06.021 (2018).

16   Bartosovic, M. & Castelo-Branco, G. Multimodal chromatin profiling using nanobody-based single-cell CUT&Tag. *bioRxiv*, 2022.2003.2008.483459, doi:10.1101/2022.03.08.483459 (2022).

17   Corces, M. R. *et al.* Single-cell epigenomic analyses implicate candidate causal variants at inherited risk loci for Alzheimer's and Parkinson's diseases. *Nat Genet* **52**, 1158-1168, doi:10.1038/s41588-020-00721-x (2020).

18   Franjic, D. *et al.* Transcriptomic taxonomy and neurogenic trajectories of adult human, macaque, and pig hippocampal and entorhinal cells. *Neuron* **110**, 452-469 e414, doi:10.1016/j.neuron.2021.10.036 (2022).

19   La Manno, G. *et al.* RNA velocity of single cells. *Nature* **560**, 494-498, doi:10.1038/s41586-018-0414-6 (2018).

20   Lavado, A. & Oliver, G. Prox1 expression patterns in the developing and adult murine brain. Developmental Dynamics 236, 518-524, doi.org/10.1002/dvdy.21024 (2007).

21   Chen, A. F. *et al.* NEAT-seq: simultaneous profiling of intra-nuclear proteins, chromatin accessibility and gene expression in single cells. *Nat Methods* **19**, 547-553, doi:10.1038/s41592-022-01461-y (2022).

22   Navarro, J. F., Sjostrand, J., Salmen, F., Lundeberg, J. & Stahl, P. L. ST Pipeline: an automated pipeline for spatial mapping of unique transcripts. *Bioinformatics* **33**, 2591-2593, doi:10.1093/bioinformatics/btx211 (2017).

23   Stuart, T., Srivastava, A., Madad, S., Lareau, C. A. & Satija, R. Single-cell chromatin state analysis with Signac. *Nat Methods* **18**, 1333-1341, doi:10.1038/s41592-021-01282-5 (2021).

24   Butler, A., Hoffman, P., Smibert, P., Papalexi, E. & Satija, R. Integrating single-cell transcriptomic data across different conditions, technologies, and species. *Nat Biotechnol* **36**, 411-420, doi:10.1038/nbt.4096 (2018).

25   Hao, Y. *et al.* Integrated analysis of multimodal single-cell data. *Cell* **184**, 3573-3587 e3529, doi:10.1016/j.cell.2021.04.048 (2021).

26   Granja, J. M. *et al.* ArchR is a scalable software package for integrative single-cell chromatin accessibility analysis. *Nat Genet* **53**, 403-411, doi:10.1038/s41588-021-00790-6 (2021).

Declarations

Acknowledgments

Contributions

Conceptualization: R.F.; Methodology: D.Z., Y.D., and Y.L.; Experimental Investigation: D.Z., Y.D.; Data Analysis: D.Z., Y.D., P.K., M.B., S.M., G.C.-B., and R.F.; Resources: P.K., G.S., S.B., Y.X., K.W.L., G.B.R., A.J.D., J.J.M., and M.B.; Original Draft: D.Z., Y.D., and R.F. All authors reviewed, edited, and approved the manuscript.

Competing interests

R.F. and Y.D. are inventors of a patent application related to this work. R.F. is scientific founder and advisor of IsoPlexis, Singleron Biotechnologies, and AtlasXomics. The interests of R.F. were reviewed and managed by Yale University Provost's Office in accordance with the University's conflict of interest policies. The remaining authors declare no competing interests.
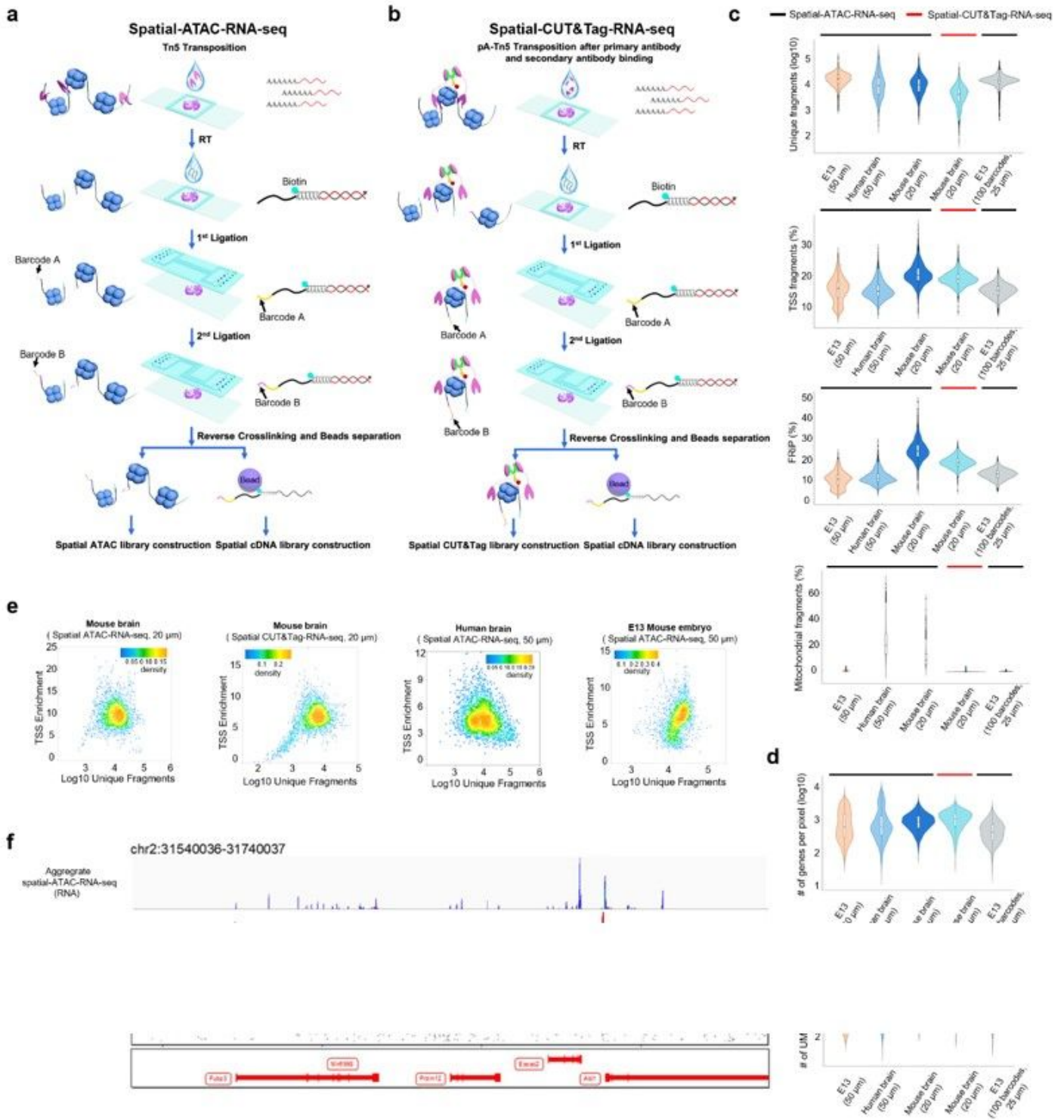
Figures

Figure 1

Spatial-ATAC-RNA-seq and spatial-CUT&Tag-RNA-seq: design, workflow, and data quality. a, b, Schematic workflow. c, Comparison of number of unique fragments, TSS fragments, fraction of reads in peaks (FRiP), and fraction of mitochondrial fragments between spatial-ATAC-RNA-seq and spatial-CUT&Tag-RNA-seq. d, Gene and UMI count distribution between spatial-ATAC-RNA-seq and spatial-CUT&Tag-RNA-seq. e, Scatterplot showing the TSS enrichment score *vs* unique nuclear fragments per cell in mouse

brain, human brain, and E13 mouse embryo. **f,** Aggregate spatial chromatin accessibility and RNA profiles in mouse brain.
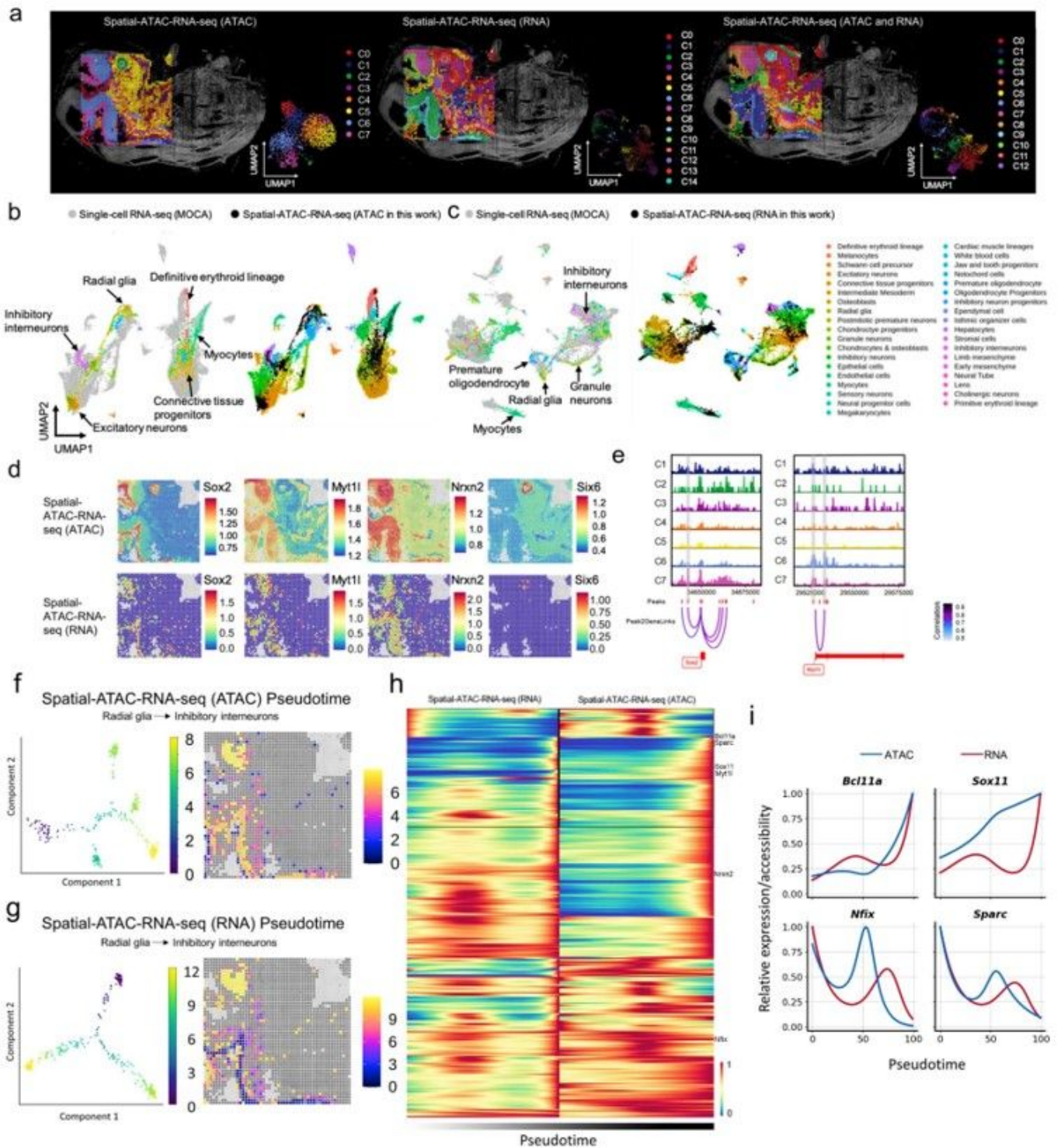

Figure 2

Spatial chromatin accessibility and transcriptome co-sequencing of E13 mouse embryo. a, Spatial map and UMAP of all the clusters for ATAC, RNA, and joint clustering of ATAC and RNA data (50 mm pixel size). Overlay of clusters with the tissue image reveals that the spatial clusters precisely match the anatomic regions. Pixel size 50 µm. **b,** Integration of scRNA-seq from E13.5 mouse embryos and ATAC data in spatial ATAC-RNA-seq. **c,** Integration of scRNA-seq from E13.5 mouse embryos and RNA data in spatial-ATAC-RNA-seq. **d,** Spatial mapping of gene scores for selected marker genes in different clusters for ATAC and RNA in spatial-ATAC-RNA-seq. **e,** Dynamics of chromatin accessibility of individual regulatory elements at *Sox2, Myt1l, Nrxn2,* and *Six6*. **f, g** Pseudotime analysis of Radial glia and inhibitory interneurons from ATAC and RNA data. **h,** The relative expression levels of genes along the pseudotime trajectory. **i,** Examples of dynamic changes of chromatin accessibility and gene expression during the pseudotime.
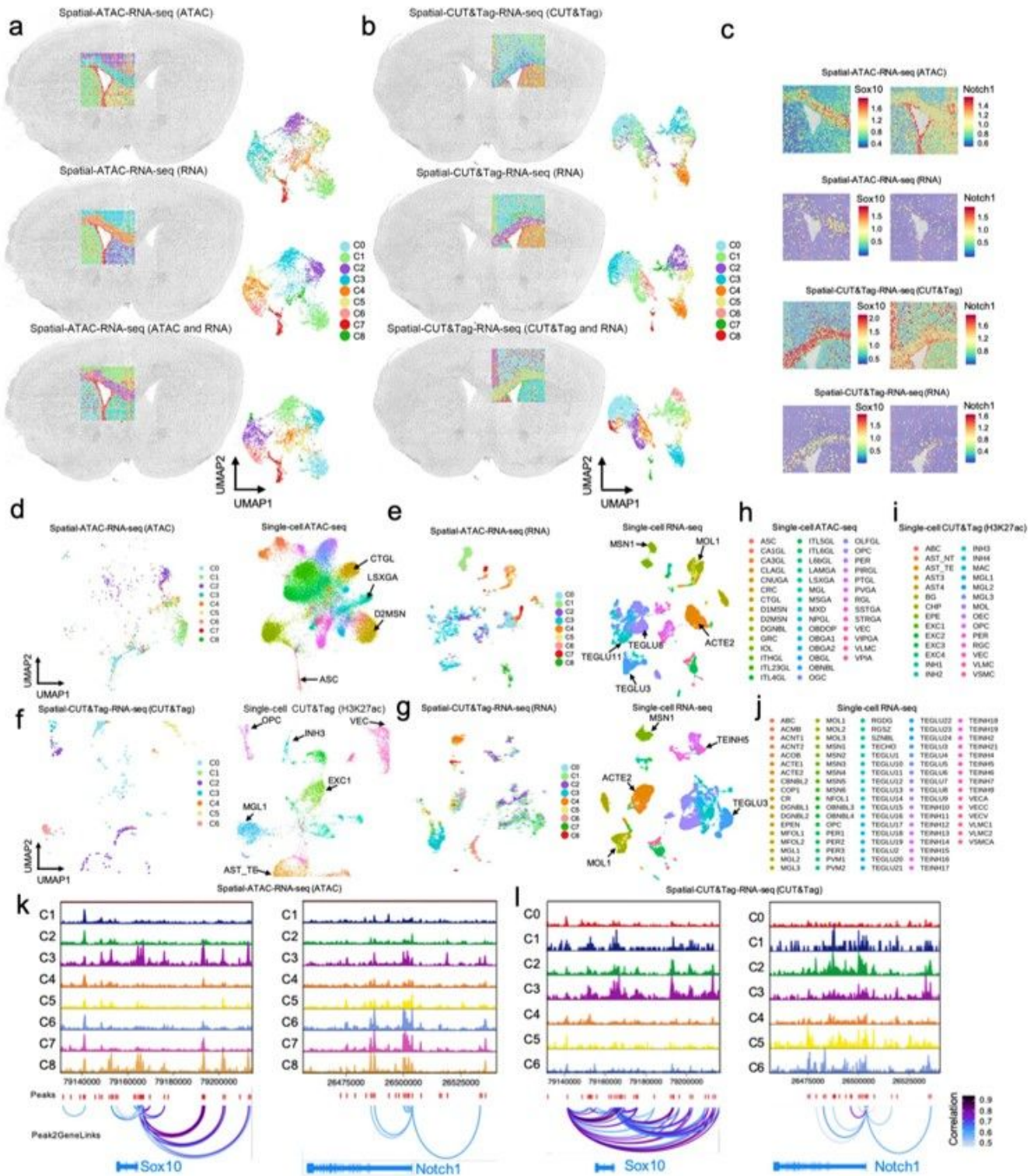
Figure 3

Spatial epigenome and transcriptome co-sequencing and integrative analysis of P21 mouse brain. a, Spatial map and UMAP of all the clusters for ATAC, RNA, and joint clustering of ATAC and RNA data in the mouse brain. Pixel size 20 μm. **b,** Spatial map and UMAP of all the clusters for CUT&Tag, RNA, and integration of CUT&Tag and RNA data in the mouse brain. Pixel size 20 μm. **c,** Spatial mapping of gene scores for selected marker genes in different clusters. **d,** Integration of scATAC-seq from mouse brains

and ATAC data in spatial-ATAC-RNA-seq. **e,** Integration of scRNA-seq from mouse brains and RNA data in spatial-ATAC-RNA-seq. **f,** Integration of scCUT&Tag (H3K27ac) from mouse brains and CUT&Tag data in spatial-CUT&Tag-RNA-seq. **g,** Integration of scRNA-seq from mouse brains and RNA data in spatial-CUT&Tag-RNA-seq. **h,** List of cell types in scATAC-seq. **i,** List of cell types in scCUT&Tag (H3K27ac). **j,** List of cell types in scRNA-seq. **k,** Dynamics of chromatin accessibility of individual regulatory elements at *Sox10*, and *Notch1*. **l,** Dynamics of histone modification of individual regulatory elements at *Sox10*, and *Notch1*. Scale bar, 1 mm.
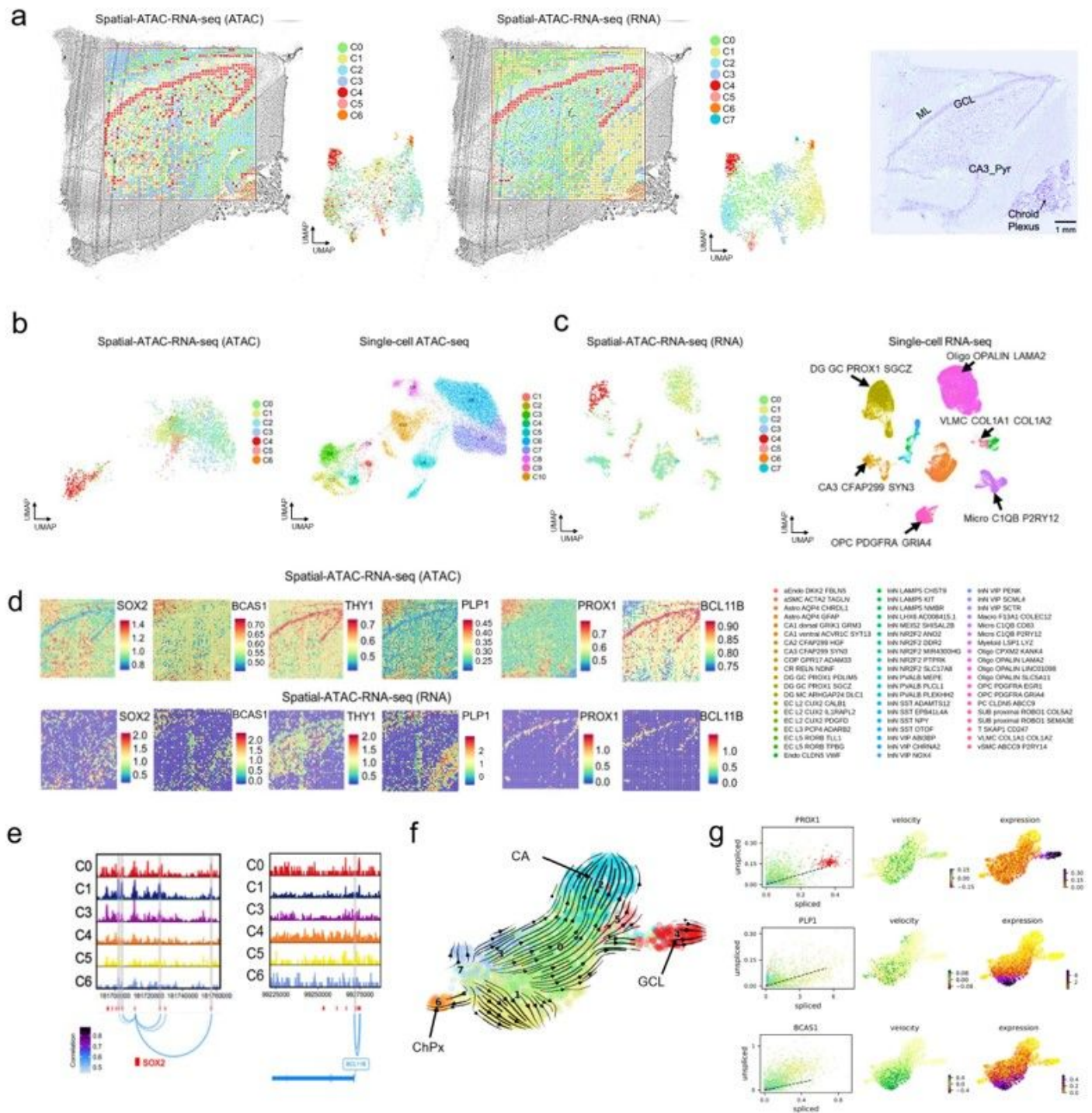

Figure 4

Spatial chromatin accessibility and transcriptome co-sequencing of human hippocampus with 50 μm pixel size. a, Spatial map (pixel size 50 μm.) and UMAP of all the clusters based on ATAC and RNA, respectively, in the human hippocampus (ML: molecular layer). **b,** Integration of scATAC-seq from human hippocampus and ATAC data in spatial-ATAC-RNA-seq. **c,** Integration of scRNA-seq from human brains and RNA data in spatial-ATAC-RNA-seq. **d,** Spatial mapping of gene scores for selected marker genes in different clusters. **e,** Dynamics of chromatin accessibility of individual regulatory elements at *SOX2,* and *BCL11B*. **f,** RNA velocity in the human hippocampus. **g**, Phase plot for selected genes (left). UMAP embedding colored by velocity (middle) and gene expression (right).

Supplementary Files

This is a list of supplementary files associated with this preprint. Click to download.

- SupplementaryInformationDi202262RF1.pdf